ePublishing

ΕΘΝΙΚΟ ΚΕΝΤΡΟ ΤΕΚΜΗΡΙΩΣΗΣ
EKT NATIONAL DOCUMENTATION CENTRE

Technical Annals

Vol 1, No 7 (2024)

Technical Annals

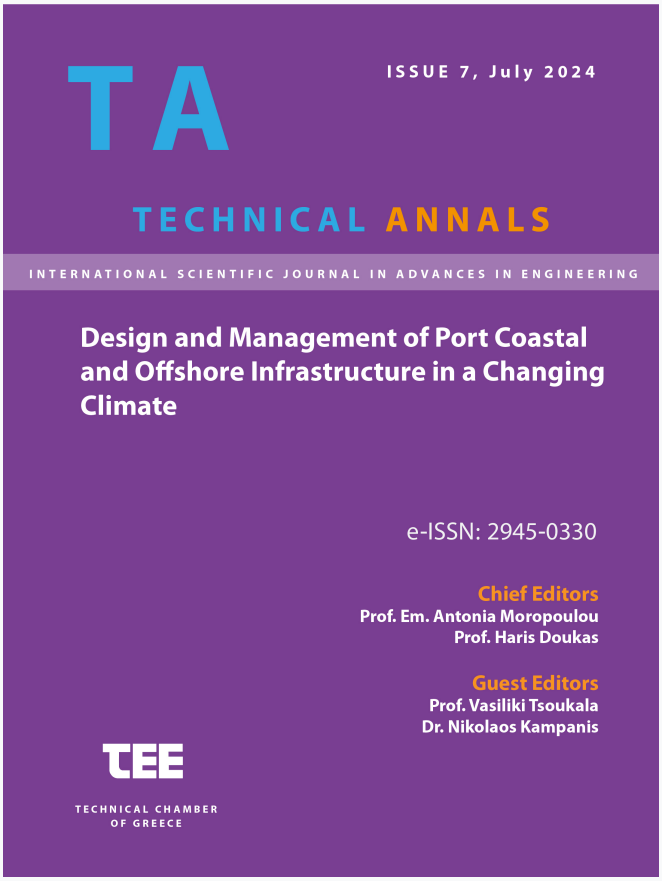

Wave climate conditions of the MUSAN underwater park in Ayia Napa with emphasis in extreme events

Georgios V. Kozyrakis, Andreas Nikolaidis, George Zodiatis, George Galanis, George Alexandrakis, Vassiliki Metheniti, Antonios Parasyris, Nikolaos A. Kampanis

doi: 10.12681/ta.40032

Copyright © 2024, Georgios V. Kozyrakis, Andreas Nikolaidis, George Zodiatis, George Galanis, George Alexandrakis, Vassiliki Metheniti, Antonios Parasyris, Nikolaos A. Kampanis

This work is licensed under a Creative Commons Attribution-NonCommercial-ShareAlike 4.0.

To cite this article:

Kozyrakis, G. V., Nikolaidis, A., Zodiatis, G., Galanis, G., Alexandrakis, G., Metheniti, V., Parasyris, A., & Kampanis, N. A. (2024). Wave climate conditions of the MUSAN underwater park in Ayia Napa with emphasis in extreme events. *Technical Annals*, *1*(7). https://doi.org/10.12681/ta.40032

https://epublishing.ekt.gr | **e-Publisher:** EKT | **Downloaded at:** 10/09/2026 10:02:44

Wave climate conditions of the MUSAN underwater park in Ayia Napa with emphasis in extreme events

Georgios V. Kozyrakis[1[0000-0002-5896-6102]], Andreas Nikolaidis[2,3[0000-0001-6214-8009]], George Zodiatis[2[0000-0003-2564-2686]], George Galanis[4[0000-0003-0620-9377]], George Alexandrakis[1[0000-0003-3690-3159]], Vassiliki Metheniti[1[0000-0003-2154-5563]], Antonios Parasyris[1[0000-0001-9498-7245]], Nikolaos A. Kampanis[1[0000-0001-6231-7730]]

[1]Coastal & Marine Research Lab, Foundation for Research and Technology, N. Plastira 100, Vassilika Vouton, GR-70013, Heraklion, Crete, Hellas
[2]ORION Research, Nicosia, Cyprus
[3]MARE INVESTIGATIORUM STUDIA (MIST) Ltd, Nicosia, Cyprus
[4]Hellenic Naval Academy Mathematical Modeling and Applications Lab, Athens, Hellas
gkoz@iacm.forth.gr

Abstract. The wave parameters in the MUSAN underwater park in Ayia Napa, Cyprus http://www.musan.com.cy/en/home were examined for a period of 5 months, December 2021 to April 2022, by means of numerical analysis tools based on the application of a nested Delft3D-WAVE (SWAN wave model) targeting the near coastal sea area. The implemented wave model used an ultra-high-resolution bathymetry of 5m, which was constructed based on local Lidar observations and EMODnet bathymetry data. The SKIRON forecasting high frequency winds and the CYCOFOS forecasting waves were used, respectively for surface forcing and lateral boundaries. The analysis of the obtained wave parameters, as well as of the wave induced forces-pressure over 4 sites closely surrounding the MUSAN underwater park in Ayia Napa demonstrate that seven extreme wave events occurred during the examined period, one in December 2021, four in January 2022 and two in March 2022. Each extreme wave event lasted for a time of few hours, with maximum SWH between 2.50 to 3.30m and maximum wave induced pressure at the sea surface between 220 to 354kPa. At the subsurface water layers during the extreme wave events, the wave induced pressure in general is decreased, where at the water depth of 2m the maximum wave induced pressure varied between 200 to 299kPA, while at the water depth of 4m the maximum wave induced pressure varied between 180 to 270kPa. The local authorities responsible for the MUSAN underwater park, after the accomplishment of the present study confirmed that the damages of the underwater structures of the park were caused during the wave extreme events in December 2021.

Keywords: extreme wave event, numerical modeling, wave forecasting.

1 Introduction

Recent developments and advances in the environmental sciences have increased the interest and the necessity for systems able to accurately monitor and simulate met-ocean

parameters. The main tools that the researcher have available today to respond adequately to the above issues are the observation networks, that record the evolution of the parameters of interest, and the numerical models which simulate their evolution in time and space. The level of difficulty in observational approaches increases when focusing on sea wave characteristics due to the lack of observational networks able to provide systematic records of the wave characteristics at a sufficient resolution. This fact underlines the importance of wave modeling systems coupled with atmospheric modeling data. Nowadays, with the development of the operational oceanography at regional and sub-regional scales there is quite a well coverage of the offshore wave characteristics, which periodically are validated against observational in-situ wave data, whenever are available [1], to reduce the unavoidable simulation uncertainty.

To address the coastal shallow or deep-sea areas, the downscaling approach is commonly applied, where the coastal higher resolution model is nested with the course resolution model providing the lateral and or initial boundaries conditions.

This work is implemented in response of a request by the Cyprus Department of Fisheries and Marine Research for a third-party scientific study. The work studies the wave conditions and the associated wave induced forces-pressure in the sea area of the MUSAN Ayia Napa underwater park (Fig. 1), during the winter period from December 2021 to April 2022. The analysis is based on the state-of-the-art numerical model simulations and provides estimations on the hourly (a total of 3331 hours) significant wave height, the wave base, the identification, and the definition of the magnitude of the extreme wave events and their maximum wave induced forces-pressure at sea surface, at 2 and 4m water depths.

Therefore, to obtain robust numerical statistics on the wave conditions in the shallow coastal area of MUSAN Ayia Napa underwater park, the identification of the extreme wave events and of the associated wave induced forces-pressure, the current numerical simulations were performed using the Delft3D-WAVE (SWAN wave model) at a very high horizontal resolution of 5m. For the implementation of the wave model in the area of interest the surface forcing from the SKIRON hourly winds, the lateral boundaries from the CYCOFOS WAM hourly waves [1-3], the local bathymetric Lidar data from the Cyprus Department of Survey and Land and the bathymetric data from the EMODnet portal were used. The CYCOFOS WAM wave forecast model was used to perform an extended numerical simulation in the Levantine basin for a period of 10 years, covering the years 2001-2010 to investigate the mean monthly and mean interannual variability of the wave characteristics toward the examination and evaluation of the wave energy potential of the area [1] (Fig. 2).

The contents of the current work involve the data sources description with respect to the bathymetry and met-ocean input data in the following chapter (chapter 2). It is followed by the mathematical description on the wave model in chapter 3 accompanied by the setup, boundary and initial conditions of the problem. Chapter 4 discusses the results for the wave distribution in different water depths and the enacting forces and pressure on specific site positions and chapter 5 provides the conclusions and a summary of the project.

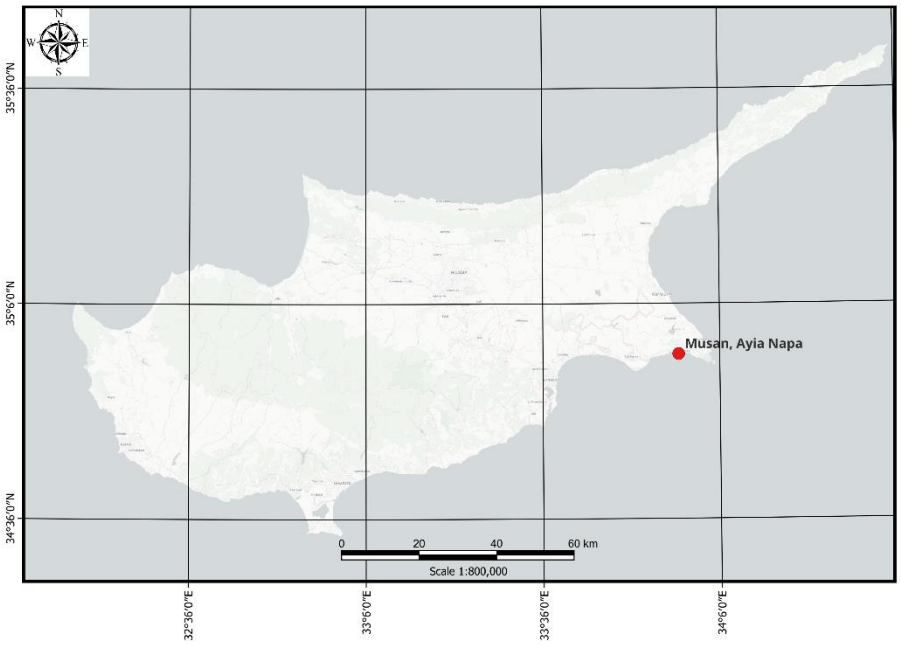

Fig. 1. MUSAN Ayia Napa underwater park coastal location. Horizontal units: degrees, minutes, seconds (WGS84).

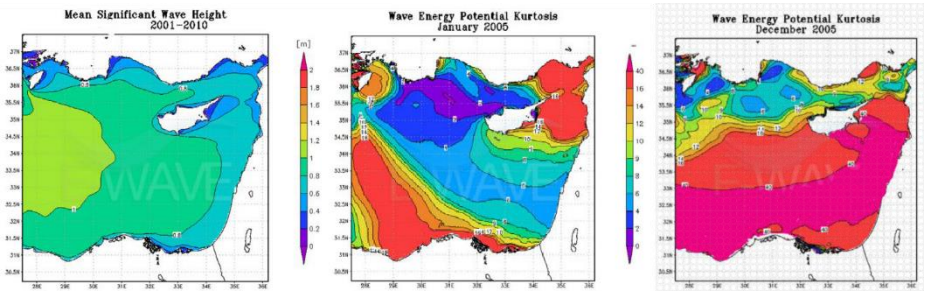

Fig. 2. Example of the wave characteristics from the numerical simulations in the Levantine basin [1]: left is the mean SWH for the years 2001-2010, middle and right are the wave energy potential Kurtosis for January and December 2005, indicating that its distribution contains extreme values, that is also applied to the broader offshore sea area of Ayia Napa.

2 Data Sources and Description: bathymetry and met-ocean data

The met-ocean and bathymetric data originated from open-source libraries and databases such as: (i) Eta/Skiron Regional Forecasting Model of the National and Kapodistrian University of Athens, School of Science, Department of Physics, Division

of Environment Physics – Meteorology, Atmospheric Modeling and Weather Forecasting Group. (ii) CYCOFOS WAM: Cyprus coastal ocean forecasting and observing system [1-5]. (iii) EMODNET Physics Portal (http://www.emodnet-physics.eu/Portal) and the EMODnet-Bathymetry portal (http://www.emodnet-bathymetry.eu/home), [6]. (iv) Lidar high-resolution bathymetry provided by the Department of Lands and Surveys, Ministry of Interior, Republic of Cyprus (Fig. 3).

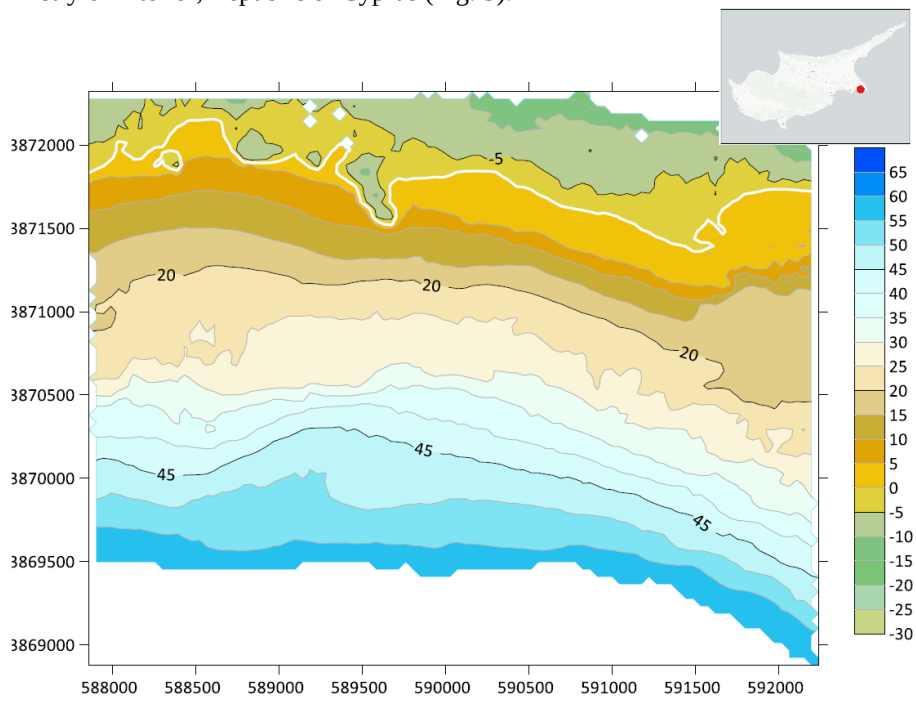

Fig. 3. Ayia Napa local high-resolution bathymetry based on 10m grid resolution (source: Department of Lands and Surveys, Ministry of Interior, Republic of Cyprus). Positive values imply increasing depths; negative values imply above sea level terrestrial elevation. Vertical units: meters; Horizontal units: meters (under WGS 84 / UTM zone 36N - EPSG:32636).

The Ayia Napa local bathymetry is based on a 10m resolution spatial grid (source: Department of Lands and Surveys, Ministry of Interior, Republic of Cyprus). The data were compared to other bathymetric distributions for validity [6,7]. No corrections were required to the original data, since the spatial distribution of the input grid points is fairly smooth without perturbations. In Fig. 3, positive values imply increasing depths; negative values imply above sea level elevation. Based on the bathymetry shown in Fig. 3, the computational seabed 5m resolution grid of Fig. 4 was constructed via interpolation and used hereafter for the wave numerical simulations.

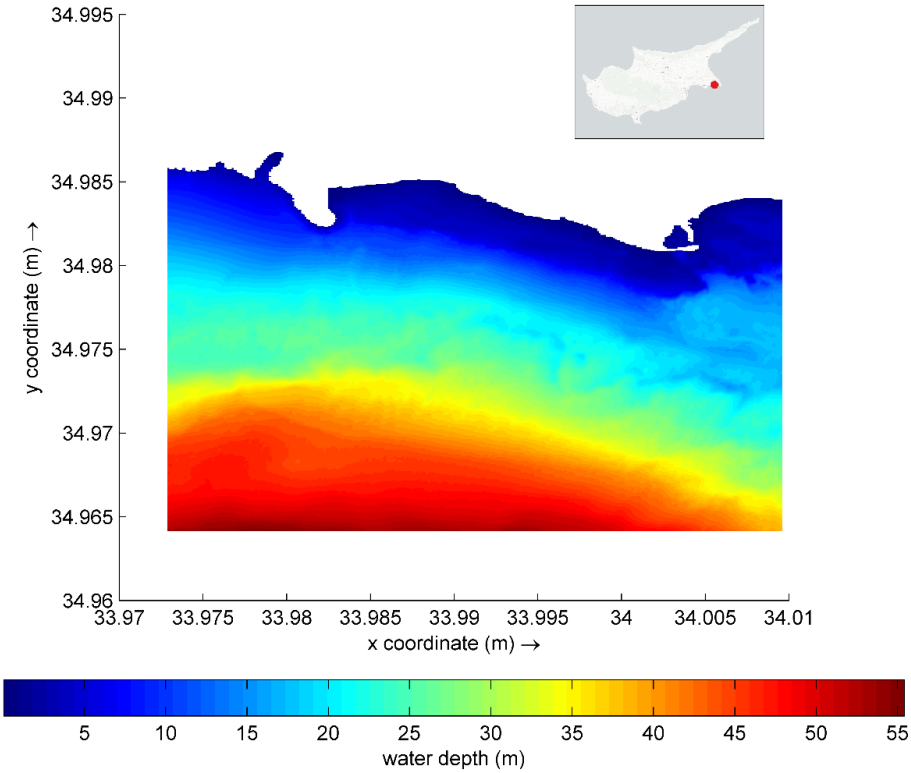

Fig. 4. Ayia Napa 5m resolution numerical domain. Positive values imply increasing depths. Vertical units: meters; Horizontal units: Decimal degrees (WGS84).

The NetCDF file format is used for the geo-spatial and marine data where possible. The Network Common Data Form (NetCDF) is an interface to a library of data access functions for storing and retrieving data in the form of arrays. Each NetCDF array is an n-dimensional (where n is 0, 1, 2, ...) rectangular structure containing items which all have the same data type (e.g., 8-bit character, 32-bit integer, etc). A scalar (simple single value) is a 0-dimensional array. In order to manipulate large NetCDF files the open-access NCO toolkit [8] has be used under Linux to support big-data operations. The NCO toolkit manipulates and analyzes data stored in NetCDF-accessible formats. It exploits the geophysical expressivity of many CF (Climate & Forecast) metadata conventions, the flexible description of physical dimensions translated by UDUnits, the network transparency of OPeNDAP, the storage features (e.g., compression, chunking, groups) of HDF (the Hierarchical Data Format) and many powerful mathematical and statistical algorithms of GSL (the GNU Scientific Library). The associated metadata are stored in the project's database and relevant queries can be performed by setting up and using MySQL schemas [9]. The use of the NetCDF file format ensures the compatibility to a very large number of pre- and post-processing software. Additionally, the data are kept as a structured block on a unique database with predefined metadata description.

2.1 Data Sources Inventory and Description

In terms of data/modelling products use, the project incorporated data from the Eta/Skiron Regional Forecasting Model of the National & Kapodistrian University of Athens, and the CYCOFOS: Cyprus coastal ocean forecasting and observing system [2-5, 10]. The computational model uses the wave modelling products as input data/parameters. The wave data for the corresponding validation periods are acquired from CYCOFOS WAM model. These are wave hindcast products composed by hourly wave parameters at 1/24° horizontal resolution (approximately 4.6km), covering the offshore region of the Ayia Napa coastal area. The hindcast product variables are summarized in Table 1.

Table 1. Main wave parameters and units in SI.

Parameter	Unit (SI)
Spectral Significant Wave Height (Hm0)	m
Wave Period at Spectral Peak / Peak Period (Tp)	s
Spectral Moments (-1,0) Wave Period (Tm-10)	s
Spectral Moments (0,2) Wave Period (Tm02)	s
Mean Wave Direction from (Mdir)	degrees
Spectral Significant Wind Wave Height	m
Spectral Moments (0,1) Wind Wave Period	S
Mean Wind Wave Direction from	degrees
Spectral Significant Primary Swell Wave Height	m
Spectral Significant Secondary Swell Wave Height	m
Spectral Moments (0,1) Primary Swell Wave Period	s
Spectral Moments (0,1) Secondary Swell Wave Period	s
Mean Primary Swell Wave Direction from	degrees
Mean Secondary Swell Wave Direction from	degrees
Wave Principal Direction at Spectral Peak	degrees
Stokes Drift U	m s^{-1}
Stokes Drift V	m s^{-1}

3 Delft3D-WAVE Model

To simulate the evolution of random, short-crested wind-generated waves in estuaries, tidal inlets, lakes etc., the third-generation SWAN model (Simulating WAves Nearshore model) has been applied for the present project.

This SWAN model is the successor of the stationary second-generation HISWA model. The main characteristics of SWAN with respect to the physics and numeric are: (i) The physics in SWAN are explicitly represented with state-of-the-art formulations. (ii) The SWAN model is fully spectral in frequencies and directions (0º – 360º). (iii) The wave computations in SWAN are unconditionally stable due to the fully implicit schemes that have been implemented. (iv) The computational grid in SWAN has not to be oriented in the mean wave direction and so the grid can handle all wave directions.

Additional aspects, which may be of importance in practical applications of the Delft3D-WAVE module, are: (i) SWAN can perform computations on a curvilinear grid. (ii) The wave forces can also be computed on the gradient of the radiation stress tensor (rather than on the dissipation rate as in the HISWA model) (iii) Output can be generated in terms of one- and two-dimensional wave spectra.

3.1 Action balance equation

In SWAN model the waves are described with the two-dimensional wave action density spectrum, even when non-linear phenomena dominate (e.g., in the surface zone). The rational for using the spectrum in such highly non-linear conditions is that, even in such conditions it seems possible to predict with reasonable accuracy this spectral distribution of the second order moment of the waves. The spectrum that is considered in SWAN is the action density spectrum $N(\sigma,\vartheta)$ rather than the energy density spectrum $E(\sigma,\vartheta)$ since in the presence of currents, action density is conserved whereas energy density is not. The independent variables are the relative frequency σ (as observed in a frame of reference moving with the current velocity) and the wave direction ϑ (the direction normal to the wave crest of each spectral component). The action density is equal to the energy density divided by the relative frequency: $N(\sigma,\vartheta) = E(\sigma,\vartheta)/\sigma$. In SWAN this spectrum may vary in time and space.

In SWAN the evolution of the wave spectrum is described by the spectral action balance equation which for Cartesian coordinates is [11]:

$$\frac{\partial}{\partial t}N + \frac{\partial}{\partial x}c_x N + \frac{\partial}{\partial y}c_y N + \frac{\partial}{\partial \sigma}c_\sigma N + \frac{\partial}{\partial \theta}c_\theta N = \frac{S}{\theta} \qquad (1)$$

The first term in the left-hand side of this equation represents the local rate of change of action density in time, the second and third term represent propagation of action in geographical space (with propagation velocities c_x and c_y in x- and y-space, respectively). The fourth term represents shifting of the relative frequency due to variations in depths and currents (with propagation velocity c_σ in σ-space). The fifth term represents depth-induced and current-induced refraction (with propagation velocity c_ϑ in ϑ-space). The expressions for these propagation speeds are taken from linear wave theory [12]. The term S (= $S(\sigma,\vartheta)$) at the right-hand side of the action balance equation is the source term in terms of energy density representing the effects of generation, dissipation and non-linear wave-wave interactions. A brief summary of the formulations that are used for the various source terms in SWAN is given below. The following processes are accounted for in SWAN: (i) generation by

wind, (ii) dissipation by white capping, (iii) bottom friction and depth-induced breaking, (iv) non-linear wave-wave interaction (quadruplets and triads).

Transfer of wind energy to the waves is described in SWAN with a resonance mechanism and a feedback mechanism. The corresponding source term for these mechanisms is commonly described as the sum of linear and exponential growth:

$$S_{in}(\sigma,\theta) = A + BE(\sigma,\theta) \tag{2}$$

in which A and B depend on wave frequency and direction, and wind speed and direction. The effects of currents are accounted for in SWAN by using the apparent local wind speed and direction. The expression for the term A is due to [13] with a filter to avoid growth at frequencies lower than the Pierson-Moskowitz frequency. Two optional expressions for the coefficient B are used in the model. The first is taken from an early version of the WAM model (known as WAM Cycle 3) [14].

The drag coefficient to relate $U*$ to the driving wind speed at 10m elevation U10 is taken from [15]. The second expression for B in SWAN is taken from the most recent version of the WAM model (known as WAM Cycle 4, [11]). It is due to the work of Cavaleri & Malanotte-Rizzoli [13] and it accounts explicitly for the interaction between the wind and the waves by considering atmospheric boundary layer effects and the roughness length of the sea surface. The corresponding set of equations is solved (as in the WAM model) with an iterative procedure.

The boundary conditions in SWAN, both in geographic and spectral space are fully absorbing for wave energy that is leaving the computational domain or crossing a coast line. The incoming wave energy along open geographic boundaries needs to be prescribed by the user. For coastal regions such incoming energy is usually provided only along the deep-water boundary and not along the lateral geographic boundaries (i.e., the spectral densities are assumed to be zero). This implies that such erroneous lateral boundary conditions are propagated into the computational area. The affected areas are typically triangular regions with the apex at the corners between the deep-water boundary and the lateral boundaries, spreading towards shore at an angle of 30º to 45º (for wind sea conditions) on either side of the deep-water mean wave direction (less for swell conditions; this angle is essentially equal to the one-sided width of the directional distribution of the incoming wave spectrum). For this reason, the lateral boundaries should be sufficiently far away from the area of interest to avoid the propagation of this error into the area.

3.2 Wave induced forces

The enacting wave-induced forces per unit surface area is the gradient of the radiation stresses in the x- and y- directions and defined by:

$$F_x = -\frac{\partial S_{xx}}{\partial x} - \frac{\partial S_{xy}}{\partial y}, and\ F_y = -\frac{\partial S_{yx}}{\partial x} - \frac{\partial S_{yy}}{\partial y} \tag{3}$$

where S is the radiation stress tensor defined by:

$$S_{xx} = \rho g \int \left(n\cos^2\theta + n - \frac{1}{2} \right) E d\sigma d\theta \quad (4)$$

$$S_{xy} = S_{yx} = \rho g \int (n \sin\theta \cos\theta) E d\sigma d\theta \quad (5)$$

$$S_{yy} = \rho g \int \left(n\sin^2\theta + n - \frac{1}{2} \right) E d\sigma d\theta \quad (6)$$

where n is the ratio of group velocity over phase velocity and $E(\sigma,\theta)$ is the energy density spectrum.

3.3 Time-varying and space-varying wave boundary conditions

In Delft3D-WAVE, time series of wave boundary conditions have been implemented using the CYCOFOS WAM model data at multiple time points.

The following example in Table 2 shows a scenario of spatial-varying and time-varying wave boundary conditions. For each boundary, different parameters such as wave height, period, direction, dir. spreading could be defined at different time points. Here a multiple time-varying and space-varying wave boundary conditions is given as reference. Note that the wind field is not defined here and is provided separately at gridded field data (U10, V10 variables) at each time-step.

Table 2. Example setup of spatial-varying and time-varying wave boundary conditions in DELFT3D-WAVE

[WaveFileInformation]	
FileVersion	= 02.00 [General]
ProjectName	= MUSAN
ProjectNr	= 1
Description	=
Description	= fnl run
OnlyInputVerify	= FALSE
SimMode	= stationary
DirConvention	= nautical
ReferenceDate	= 2022-1-5
TSeriesFile	= timeseries.bcw
[TimePoint]	
Time	=6.00E+01
WaterLevel	=0.00E+00
XVeloc	=0.00E+00
YVeloc	=0.00E+00
WindSpeed	=
WindDir	=
[TimePoint]	
Time	=1.20E+02
WaterLevel	=0.00E+00
XVeloc	=0.00E+00
YVeloc	=0.00E+00
WindSpeed	=
WindDir	=
[TimePoint]	
Time	=1.80E+02
WaterLevel	=0.00E+00
XVeloc	=0.00E+00
YVeloc	=0.00E+00
WindSpeed	=
WindDir	=
[TimePoint]	
Time	=2.40E+02
WaterLevel	=0.00E+00
XVeloc	=0.00E+00
YVeloc	=0.00E+00
WindSpeed	=
WindDir	=
[TimePoint]	
Time	=3.00E+02
… etc	

[Boundary]	
Name	= Boundary West
Definition	= xy-coordinates
StartCoordX	=5.00E+05
EndCoordX	=5.00E+05
StartCoordY	=4.93E+06
EndCoordY	=4.79E+06
SpectrumSpec	= parametric
SpShapeType	= jonswap
PeriodType	= peak
DirSpreadType	= power
PeakEnhanceFac	=3.30E+00
GaussSpread	=1.00E-02
CondSpecAtDist	=2.78E+04
CondSpecAtDist	=5.55E+04
CondSpecAtDist	=6.33E+04
CondSpecAtDist	=8.33E+04
CondSpecAtDist	=1.11E+05
CondSpecAtDist	=1.39E+05
[Boundary]	
Name	= Boundary South
Definition	= xy-coordinates
StartCoordX	=5.00E+05
EndCoordX	=6.22E+05
StartCoordY	=4.76E+06
EndCoordY	=4.76E+06
SpectrumSpec	= parametric
SpShapeType	= jonswap
PeriodType	= peak
DirSpreadType	= power
PeakEnhanceFac	=3.30E+00
GaussSpread	=1.00E-02
CondSpecAtDist	=0.00E+00
CondSpecAtDist	=1.00E+03
CondSpecAtDist	=1.00E+04
CondSpecAtDist	=2.04E+04
CondSpecAtDist	=4.08E+04
CondSpecAtDist	=6.11E+04
CondSpecAtDist	=8.15E+04
CondSpecAtDist	=1.02E+05
CondSpecAtDist	=1.22E+05
… etc	

4 Results and Discussion

The results provided in this section include four monitoring sites closely surrounding the Ayia Napa underwater park, with coordinates and bottom depth. Their coordinates are listed in Table 3 and their positions are illustrated in Fig. 5.

Table 3. MUSAN Ayia Napa underwater park numerical monitoring sites

Position No.	Decimal Degrees Longitude (WGS84)	Decimal Degrees Latitude (WGS84)	Bottom depth (m)
1	33.98403055555556°	34.98229444444445°	8.7
2	33.98378611111112°	34.98300277777778°	6.8
3	33.98378611111112°	34.98229444444445°	8.8
4	33.98403055555556°	34.98300277777778°	5.3

Fig. 5. The four numerical monitoring sites for wave parameters in the MUSAN Ayia Napa underwater park.

4.1 Significant Wave Height - SWH

The SWH time series during the examined period show (Fig. 6a; b) seven extreme wave events for all 4 numerical monitoring sites.

For the numerical monitoring *site 1* (Fig.6a: Position 1), one extreme wave event simulated in December 2021, between 19 to 20 December with maximum SWH up to 3.16m. Four extreme wave events were simulated in January 2022: one event between 9-10 January with maximum SWH up to 2.30m, a second event on the 19 January with maximum SWH 3.07m, a third event on the 23 January with maximum SWH 2.57m and a fourth event on the 25 January with maximum SWH 2.58m. Moreover, two

extreme wave events were simulated in March 2022: one event between 3-4 March with maximum SWH 3.30m and a second event between 10-11 March with maximum SWH 2.99m. Therefore, in the numerical monitoring *site 1*, maximum SWH greater than 3m were simulated in December 2021, January, and March 2022. No extreme wave event was simulated at the numerical monitoring *site 1* during February and April 2022.

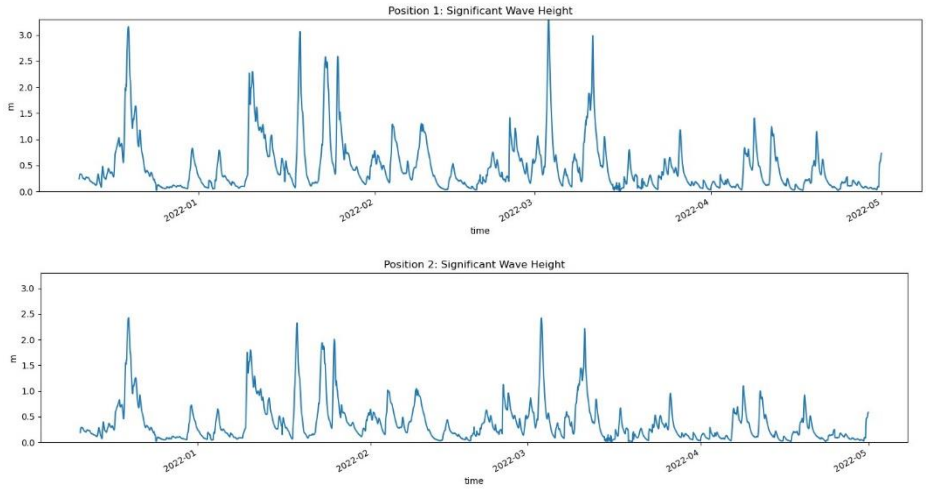

Fig. 6a. Ayia Napa Significant Wave Height (SWH) timeseries at the first and second numerical monitoring sites, 11 December 2021 to 30 April 2022.

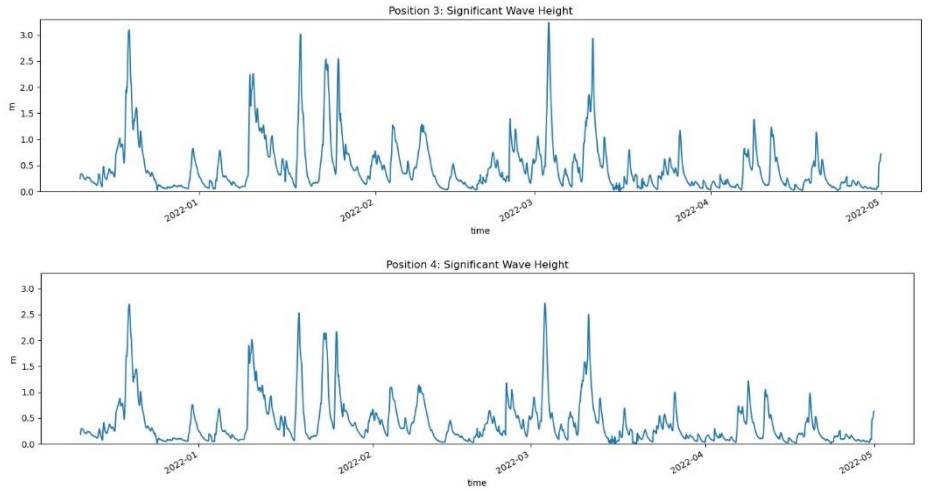

Fig. 6b. Ayia Napa Significant Wave Height (SWH) timeseries at the third and fourth numerical monitoring sites, 11 December 2021 to 30 April 2022.

For the numerical monitoring site 2 (Fig. 6a: Position 2), one extreme wave event was simulated in December 2021, between 19 to 20 December with maximum SWH up to 2.40m. Four extreme wave events were spotted in January 2022: one event between 9-10 January with maximum SWH up to 1.80m, a second event on the 19 January with maximum SWH 2.33m, a third event on the 23 January with maximum SWH 1.94m and a fourth event on the 25 January with maximum SWH 1.99m. Finally, two extreme wave events were simulated in March 2022, one between 3-4 March with maximum SWH 2.42m and a second between 10-11 March with maximum SWH 2.21m.

Therefore, in the numerical monitoring site 2, maximum SWH greater than 2m was simulated in December 2021, January, and March 2022. No extreme wave events were spotted at the numerical monitoring site 2 during February and April 2022 in the area under study.

For the numerical monitoring site 3 (Fig. 6b: Position 3), one extreme wave event was simulated in December 2021, between 19 to 20th of December with maximum SWH up to 3m. Four extreme wave events were spotted during January 2022: one event between 9-10 January with maximum SWH up to 2.23m, a second event on the 19 January with maximum SWH 3m, a third event on the 23 January with maximum SWH 2.53m and a fourth event on the 25 January with maximum SWH 2.54m. Finally, two extreme wave events were simulated during March 2022: one event between 3-4 March with maximum SWH 3.24m and a second event between 10-11 March with maximum SWH 2.93m.

Therefore, in the numerical monitoring site 3, maximum SWH greater than 3m were observed in December 2021, January, and March 2022. No extreme wave event was spotted at the numerical monitoring site 3 during February and April 2022 in the area under study.

For the numerical monitoring site 4 (Fig.6b: Position 4), one extreme wave event was simulated in December 2021, between 19 to 20 December with maximum SWH up to 2.70m. Four extreme wave events spotted in January 2022, one event between 9-10 January with maximum SWH up to 2m, a second event on the 19 January with maximum SWH 2.53m, a third event on the 23 January with maximum SWH 2.11m and a fourth event on the 25 January with maximum SWW 2.15m. Two extreme wave events were simulated in March 2022, one event between 3-4 March with maximum SWH 2.72m and a second event between 10-11 March with maximum SWH 2.50m.

Therefore, in the numerical monitoring site 4, maximum SWH greater than 2.50m were spotted in December 2021, January, and March 2022. No extreme wave event occurred at the numerical monitoring site 4 during February and April 2022 in the area under study.

4.2 Wave induced forces-maximum pressure at sea surface

Similarly, to the SWH, the wave induced forces-pressure time series at sea surface during the examined period show (Fig. 7a; b) seven extreme wave induced forces-pressure events for all 4 numerical monitoring sites.

For the numerical monitoring site 1 (Fig. 7a: Position 1), one extreme event was simulated in December 2021, between 19 to 20 December with maximum surface pressure ($P_{s,max}$) 63kPa. Four extreme events spotted in January 2022, one event between 9-

10 January with $P_{s,max}$= 26 kPa , a second event on the 19 January with maximum pressure with $P_{s,max}$= 49 kPa , a third event on the 23 January with $P_{s,max}$= 38 kPa and a fourth event on the 25 January with $P_{s,max}$= 33kPa. Two extreme pressure events were simulated in March 2022, one event between 3-4 March with $P_{s,max}$= 65kPa and a second event between 10-11 March with $P_{s,max}$= 43kPa.

Therefore, in the numerical monitoring site 1, maximum wave induced forces-pressure greater than 50kPa spotted in December 2021 and March 2022. No extreme wave induced forces-pressure event occurred at the numerical monitoring site1 in February and April 2022 in the area under study.

For the numerical monitoring site 2, the wave induced forces-pressure time series at sea surface during the examined period show (Fig. 7a: Position 2), one extreme event was simulated in December 2021, between 19 to 20 December with $P_{s,max}$= 70 kPa. Four extreme events spotted in January 2022, one event between 9-10 January with $P_{s,max}$= 37 kPa, a second event on the 19 January with $P_{s,max}$= 60 kPa, a third event on the 23 January with $P_{s,max}$= 56 kPa and a fourth event on the 25 January with $P_{s,max}$= 38 kPa. Two extreme pressure events were simulated in March 2022, one event between 3-4 March with $P_{s,max}$= 112kPa and a second event between 10-11 March with $P_{s,max}$= 71kPa.

Therefore, in the numerical monitoring site 2, maximum wave induced forces-pressure greater than 50kPa spotted in December 2021 and March 2022. No extreme wave induced forces-pressure event occurred at the numerical monitoring site 2 in February and April 2022 in the area under study.

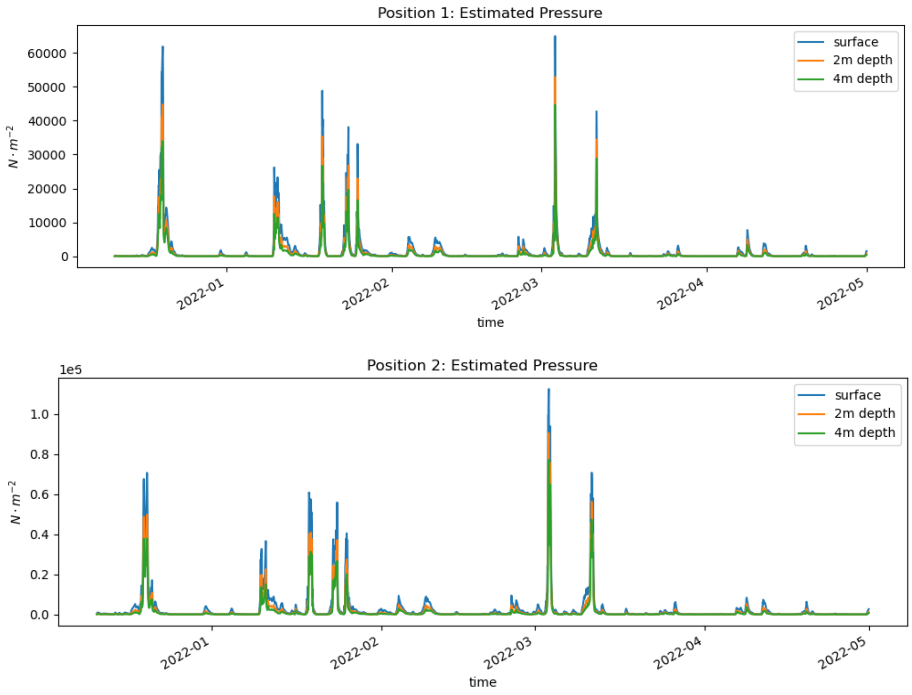

Fig. 7a. MUSAN Ayia Napa wave induced pressure at sea surface, 2m and 4m water depths, at the first and second numerical monitoring sites, 11 December 2021 to 30 April 2022.

For the numerical monitoring site 3, the wave induced forces-pressure time series at sea surface during the examined period show (Fig. 7b: Position 3), one extreme event was simulated in December 2021, between 19 to 20 December with $P_{s,max}$= 130 kPa. Four extreme events spotted in January 2022, one event between 9-10 January with $P_{s,max}$= 50kPa, a second event on the 19 January with $P_{s,max}$= 99kPa, a third event on the 23 January with $P_{s,max}$= 80kPa and a fourth event on the 25 January with $P_{s,max}$= 74 kPa. Two extreme pressure events were simulated in March 2022, one event between 3-4 March with $P_{s,max}$= 144 kPa and a second event between 10-11 March with $P_{s,max}$= 94 kPa.

Therefore, in the numerical monitoring site 3, maximum wave induced forces-pressure greater than 100kPa spotted in December 2021 and March 2022. No extreme wave induced forces-pressure event occurred at the numerical monitoring site 3 in February and April 2022.

For the numerical monitoring site 4, the wave induced forces-pressure time series at sea surface during the examined period show (Fig. 7b: Position 4), one extreme event was simulated in December 2021, between 19 to 20 December with $P_{s,max}$= 270kPa. Four extreme events spotted in January 2022, one event between 9-10 January with $P_{s,max}$= 153kPa, a second event on the 19 January with $P_{s,max}$= 227kPa, a third event on the 23 January with $P_{s,max}$= 220kPa and a fourth event on the 25 January with $P_{s,max}$=

166kPa. Two extreme pressure events were simulated in March 2022, one event between 3-4 March with $P_{s,max}$= 354kPa and a second event between 10-11 March with $P_{s,max}$= 288kPa.

Therefore, in the numerical monitoring site 4, maximum wave induced forces-pressure greater than 200kPa spotted in December 2021, January 2022 and March 2022.

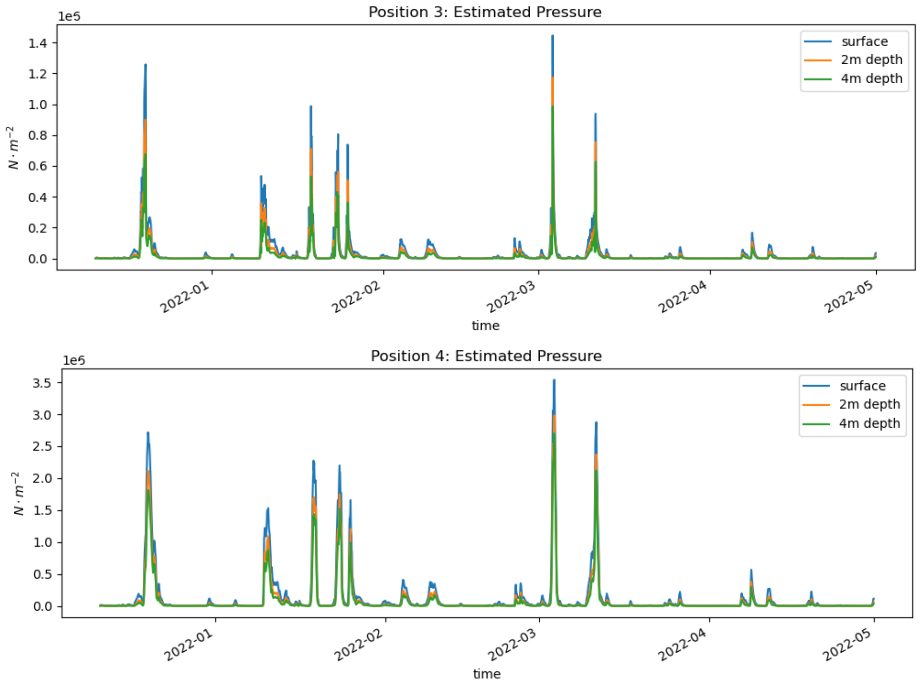

Fig. 7b. MUSAN Ayia Napa wave induced pressure at sea surface, 2m and 4m water depths, at the third and four numerical monitoring sites, 11 December 2021 to 30 April 2022.

4.3 Wave induced forces-pressure at 2m water depth

The wave induced forces-pressure time series at the 2 m water depth during the examined period show (Fig. 7a; b) seven extreme wave induced forces-pressure events for all 4 numerical monitoring sites.

For the numerical monitoring site 1, the wave induced forces-pressure time series at 2m water depth during the examined period show (Fig. 7a: Position 1), one extreme event was simulated in December 2021, between 19 to 20 December with maximum pressure ($P_{2,max}$) 45kPa. Four extreme events spotted in January 2022, one event between 9-10 January with $P_{2,max}$= 18kPa, a second event on the 19 January with $P_{2,max}$= 35kPa, a third event on the 23 January with $P_{2,max}$= 27kPa and a fourth event on the 25 January with $P_{2,max}$= 22kPa. Two extreme pressure events were simulated in March 2022, one event between 3-4 March with $P_{2,max}$= 53kPa and a second event between 10-11 March with $P_{2,max}$= 35kPa.

Therefore, in the numerical monitoring site 1, maximum wave induced forces-pressure at 2m water depth greater than 40kPa spotted in December 2021 and March 2022. No extreme wave induced forces-pressure event occurred at the numerical monitoring site1 in February and April 2022 in the area under study.

For the numerical monitoring site 2, the wave induced forces-pressure time series at 2m water depth during the examined period show (Fig. 7a: Position2), one extreme event was simulated in December 2021, between 19 to 20 December with $P_{2,max}$= 50kPa. Four extreme events spotted in January 2022, one event between 9-10 January with $P_{2,max}$= 22kPa, a second event on the 19 January with $P_{2,max}$= 41kPa, a third event on the 23 January with $P_{2,max}$= 37kPa and a fourth event on the 25 January with $P_{2,max}$= 27kPa. Two extreme pressure events were simulated in March 2022, one event between 3-4 March with $P_{2,max}$= 91kPa and a second event between 10-11 March with $P_{2,max}$= 56kPa.

Therefore, in the numerical monitoring site 2, maximum wave induced forces-pressure at 2m water depth greater than 40kPa spotted in December 2021, January and March 2022. No extreme wave induced forces-pressure event occurred at the numerical monitoring site 2 in February and April 2022.

For the numerical monitoring site 3, the wave induced forces-pressure time series at 2m water depth during the examined period show (Fig. 7b: Position 3), one extreme event was simulated in December 2021, between 19 to 20 December with $P_{2,max}$= 90kPa. Four extreme events spotted in January 2022, one event between 9-10 January with $P_{2,max}$= 36kPa, a second event on the 19 January with $P_{2,max}$= 71kPa, a third event on the 23 January with $P_{2,max}$= 56kPa and a fourth event on the 25 January with $P_{2,max}$= 51kPa. Two extreme pressure events were simulated in March 2022, one event between 3-4 March with $P_{2,max}$= 117kPa and a second event between 10-11 March with $P_{2,max}$= 75kPa.

Therefore, in the numerical monitoring site 3, maximum wave induced forces-pressure greater than 50kPa spotted in December 2021, January, and March 2022. No extreme wave induced forces-pressure event occurred at the numerical monitoring site 3 in February and April 2022 in the area under study.

For the numerical monitoring site 4, the wave induced forces-pressure time series at 2m water depth during the examined period show (Fig. 7b: Position 4), one extreme event was simulated in December 2021, between 19 to 20 December with $P_{2,max}$= 208kPa. Four extreme events spotted in January 2022, one event between 9-10 January with $P_{2,max}$= 105kPa, a second event on the 19 January with $P_{2,max}$= 167kPa, a third event on the 23 January with $P_{2,max}$= 175kPa and a fourth event on the 25 January with $P_{2,max}$= 110kPa. Two extreme pressure events were simulated in March 2022, one event between 3-4 March with $P_{2,max}$= 299kPa and a second event between 10-11 March with $P_{2,max}$= 237kPa.

Therefore, in the numerical monitoring site 4, maximum wave induced forces-pressure greater than 150kPa spotted in December 2021, January and March 2022. No extreme wave induced forces-pressure event occurred at the numerical monitoring site 4 in February and April 2022 in the area under study.

4.4 Wave induced forces-pressure at 4m water depth

The wave induced forces-pressure time series at the 4m water depth during the examined period show (Fig. 7a; b) seven extreme wave induced forces-pressure events for all 4 numerical monitoring sites.

For the numerical monitoring site 1, the wave induced forces-pressure time series at 4m water depth during the examined period show (Fig. 7a: Position 1), one extreme event was simulated in December 2021, between 19 to 20 December with maximum pressure ($P_{4,max}$) 33kPa. Four extreme events spotted in January 2022, one event between 9-10 January with $P_{4,max}$= 12kPa, a second event on the 19 January with $P_{4,max}$= 27kPa, a third event on the 23 January with $P_{4,max}$= 20kPa and a fourth event on the 25 January with $P_{4,max}$= 16kPa. Two extreme pressure events were simulated in March 2022, one event between 3-4 March with $P_{4,max}$= 45kPa and a second event between 10-11 March with $P_{4,max}$= 29kPa.

Therefore, in the numerical monitoring site 1, maximum wave induced forces-pressure at 4m water depth greater than 20kPa spotted in December 2021, January and March 2022. No extreme wave induced forces-pressure event occurred at the numerical monitoring site1 in February and April 2022 in the area under study.

For the numerical monitoring site 2, the wave induced forces-pressure time series at 4m water depth during the examined period show (Fig. 7a: Position2), one extreme event was simulated in December 2021, between 19 to 20 December with $P_{4,max}$= 37kPa. Four extreme events spotted in January 2022, one event between 9-10 January with $P_{4,max}$= 15kPa, a second event on the 19 January with $P_{4,max}$= 31kPa, a third event on the 23 January with $P_{4,max}$= 27kPa and a fourth event on the 25 January with $P_{4,max}$= 20kPa. Two extreme pressure events were simulated in March 2022, one event between 3-4 March with $P_{4,max}$= 77kPa and a second event between 10-11 March with $P_{4,max}$= 47kPa.

Therefore, in the numerical monitoring site 2, maximum wave induced forces-pressure at 4m water depth greater than 20kPa spotted in December 2021, January and March 2022. No extreme wave induced forces-pressure event occurred at the numerical monitoring site 2 in February and April 2022 in the area under study.

For the numerical monitoring site 3, the wave induced forces-pressure time series at 4m water depth during the examined period show (Fig. 7b: Position 3), one extreme event was simulated in December 2021, between 19 to 20 December with $P_{4,max}$= 67kPa. Four extreme events spotted in January 2022, one event between 9-10 January with $P_{4,max}$= 23kPa, a second event on the 19 January with $P_{4,max}$= 53kPa, a third event on the 23 January with $P_{4,max}$= 43kPa and a fourth event on the 25 January with $P_{4,max}$= 36kPa. Two extreme pressure events were simulated in March 2022, one event between 3-4 March with $P_{4,max}$= 98kPa and a second event between 10-11 March with $P_{4,max}$= 63kPa.

Therefore, in the numerical monitoring site 3, maximum wave induced forces-pressure at 4m water depth greater than 30kPa spotted in December 2021, January and March 2022. No extreme wave induced forces-pressure event was occurred at the numerical monitoring site 3 in February and April 2022 in the area under study.

For the numerical monitoring site 4, the wave induced forces-pressure time series at 4m water depth during the examined period show (Fig. 7b: Position 4), one extreme event was simulated in December 2021, between 19 to 20 December with $P_{4,max}$= 180kPa. Four extreme events spotted in January 2022, one event between 9-10 January with $P_{4,max}$= 88kPa, a second event on the 19 January with $P_{4,max}$= 140kPa, a third event on the 23 January with $P_{4,max}$= 150kPa and a fourth event on the 25 January with $P_{4,max}$= 99kPa. Two extreme pressure events were simulated in March 2022, one event between 3-4 March with $P_{4,max}$= 270kPa and a second event between 10-11 March with $P_{4,max}$= 210kPa.

Therefore, in the numerical monitoring site 4, maximum wave induced forces-pressure at 4m water depth greater than 100kPa spotted in December 2021, January and March 2022. No extreme wave induced forces-pressure event occurred at the numerical monitoring site 4 in February and April 2022 in the area under study.

4.5 Wave Base

The timeseries of the wave base values at the 4 numerical monitoring sites are quite variable and are closely connected to the variability of the wavelength (Fig. 8a; b). The maximum wave base values were computed to vary between 15 to 22m and are coincided to occur during the seven extreme waves events mentioned in the previous paragraphs. Therefore, the sea bottom of the MUSAN Ayia Napa underwater park is affected during the extreme wave events, because it is shallower compared to the maximum wave base values. Nevertheless, as from the frequency distribution of the wave base values during the entire period under examination (Fig. 9a; b), the mean average of the wave base at its maximum frequency distribution is estimated to be close to 5m.

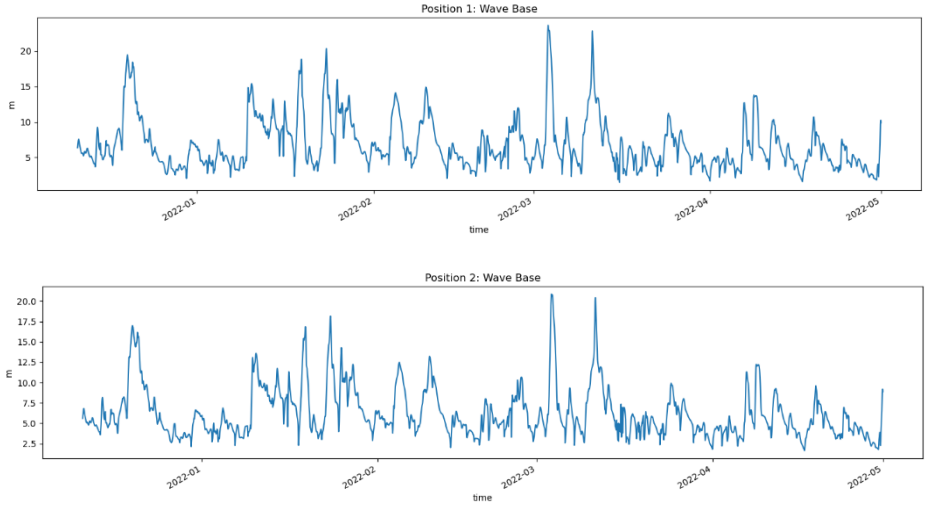

Fig. 8a. MUSAN Ayia Napa wave base at the first and second numerical monitoring sites, 11 December 2021 to 30 April 2022.

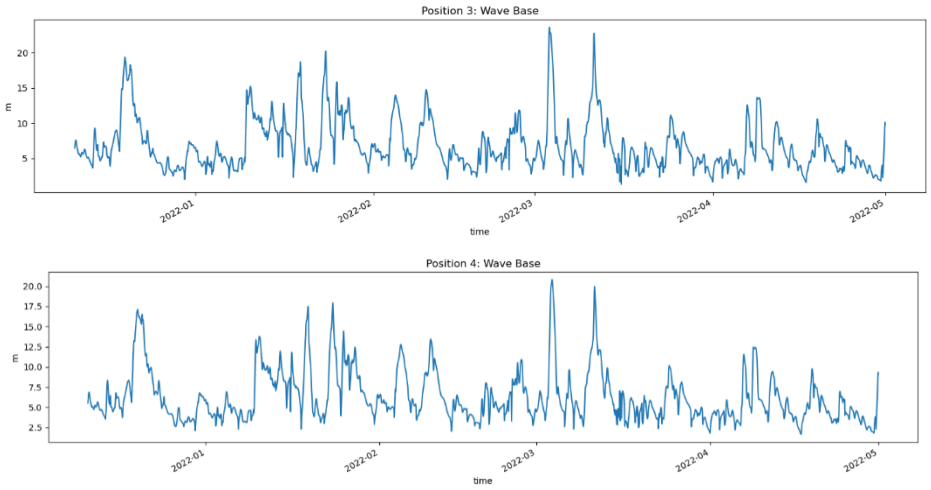

Fig. 8b. MUSAN Ayia Napa wave base at the third and four numerical monitoring sites, 11 December 2021 to 30 April 2022.

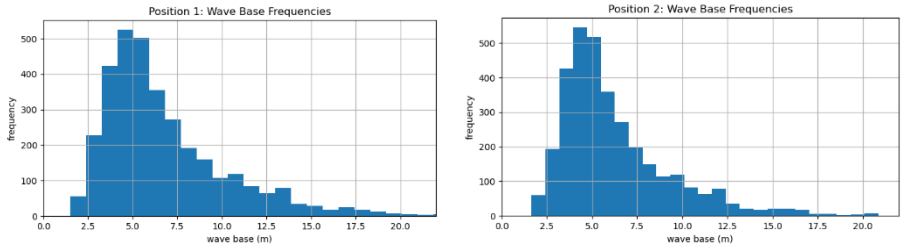

Fig. 9a. MUSAN Ayia Napa wave base frequency at the first and second numerical monitoring sites, 11 December 2021 to 30 April 2022.

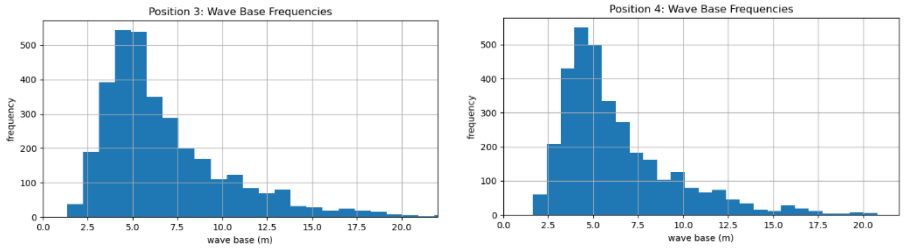

Fig. 9b. MUSAN Ayia Napa wave base frequency at the third and four numerical monitoring sites, 11 December 2021 to 30 April 2022.

5 Conclusions

The results presented and analyzed in the previous sections, based on ultra-high-resolution wave modeling over four sites surrounding the area under study, by means of state-of-the-art numerical models, prove that the MUSAN Ayia Napa underwater park was affected by seven extreme wave events during the period December 2021 to April 2022, as shown in Table 4. One event was simulated between 19-20 December 2021 while four more extreme wave events spotted in January 2022: one between 9-10 January, a second on the 19th of January, a third one on January 23 and a fourth event on the 23d of January. During March 2022, two more extreme wave events were spotted, one between 3-4 March and the second between 10-11 March.

The maximum SWH was numerically simulated during the above months at the sites 1 and 3 with values a little above than 3m, while over the sites 2 and 4 the maximum simulated SWH was simulated between 2.5 and 3m. During February and April 2022 no extreme wave events were simulated.

The maximum mean averaged wave induced forces-pressure at sea surface during the entire period of the simulations was 240kPa at the site 4, while the maximum pressure at sea surface was also found at this site with values up to 354kPa during 3-4 March 2022. Similarly, at the water depth of 2 and 4m at the same site and same period, the maximum pressure was 299kPa and 270kPa, respectively.

The maximum wave base was simulated during the seven extreme wave events with values between 15-22 m, while for the rest period the mean wave base should be considered 5m based on the wave base frequency distribution.

The local authorities responsible for the MUSAN underwater park, after the completion of the present work confirmed that the damages of the underwater structures of the park were caused during the wave extreme events in December 2021.

Table 4. The MUSAN Ayia Napa underwater park maximum SWH, wave induced forces-pressure at sea surface, 2m and 4m water depths

Site 1 **extreme wave events**	SWH m	$P_{s,max}$ (kPa)	$P_{2,max}$ (kPa)	$P_{4,max}$ (kPa)
19/12/2021	3.16	63	45	33
9-10/01/2021	2.30	26	18	12
19/01/2022	3.07	49	35	27
23/01/2022	2.57	38	27	20
25/01/2022	2.58	33	22	16
3-4/03/2022	3.30	65	53	45
10-11/03/2022	2.99	43	35	29
Mean max. average	3.07	45	33	26

Site 2	SWH m	$P_{s,max}$ (kPa)	$P_{2,max}$ (kPa)	$P_{4,max}$ (kPa)
19/12/2021	2.40	70	50	37
9-10/01/2021	1.80	37	22	15
19/01/2022	2.33	60	41	31
23/01/2022	1.94	56	37	27
25/01/2022	1.99	38	27	20
3-4/03/2022	2.42	112	91	77
10-11/03/2022	2.21	71	56	47
Mean max average	2.15	63	46	36
Site 3	SWH m	$P_{s,max}$ (kPa)	$P_{2,max}$ (kPa)	$P_{4,max}$ (kPa)
19/12/2021	3.00	130	90	67
9-10/01/2021	2.23	50	36	23
19/01/2022	3.00	99	71	53
23/01/2022	2.53	80	56	43
25/01/2022	2.54	74	51	36
3-4/03/2022	3.24	144	117	98
10-11/03/2022	2.93	94	75	63
Mean max average	3.17	96	71	55
Site4	SWH m	$P_{s,max}$ (kPa)	$P_{2,max}$ (kPa)	$P_{4,max}$ (kPa)
19/12/2021	2.70	270	208	180
9-10/01/2021	2.00	153	105	88
19/01/2022	2.53	227	167	140
23/01/2022	2.11	220	175	150
25/01/2022	2.15	166	110	99
3-4/03/2022	2.72	354	299	270
10-11/03/2022	2.50	288	237	210
Mean max average	2.39	240	186	162

Acknowledgements

The authors would like to express their gratitude to the Department of Survey and Lands for the provision of the Lidar data, and to the Department of Fisheries and Marine Research, particularly to its officer Giorgos Payiatas for his cooperation during the realisation of the study.

References

1. Zodiatis, G., et al., Wave energy potential in the Eastern Mediterranean Levantine Basin. An integrated 10-year study. Renewable Energy, 2014. 69: p. 311-323.
2. Zodiatis, G., et al. Downscaling the Copernicus CMEMS Med-MFC in the Eastern Mediterranean: The new CYCOFOS forecasting systems at regional and sub-regional scales. in Proceedings of the Eight EuroGOOS International Conference. 2017.
3. Zodiatis, G., et al. The new CYCOFOS forecasting at coastal, sub-regional and regional scales in the Mediterranean and the Black Sea. in EGU General Assembly Conference Abstracts. 2021.
4. Zodiatis, G., et al., Cyprus coastal ocean forecasting and observing system, in Elsevier Oceanography Series, H. Dahlin, et al., Editors. 2003, Elsevier. p. 36-45.
5. Zodiatis, G., et al., Operational ocean forecasting in the Eastern Mediterranean: implementation and evaluation. Ocean Sci., 2008. 4(1): p. 31-47.
6. Consortium, E.B., EMODnet Digital Bathymetry (DTM 2018). 2018.
7. Danielson, J.J. and D.B. Gesch, Global multi-resolution terrain elevation data 2010 (GMTED2010), in Open-File Report. 2011.
8. Zender, C.S., Analysis of self-describing gridded geoscience data with netCDF Operators (NCO). Environmental Modelling & Software, 2008. 23(10): p. 1338-1342.
9. Widenius, M. and D. Axmark, Mysql Reference Manual, ed. D. Paul. 2002: O'Reilly & Associates, Inc. 712.
10. Zodiatis, G., et al. OM14A-2027: Downscaling the Copernicus marine service in the Eastern Mediterranean. in Advances in Coastal Ocean Modelling, Prediction and Ocean Observing system evaluation, Ocean Science meeting, AGU 2018. 2018.
11. Komen, G.J., et al., Dynamics and modelling of ocean waves. 1996: Cambridge university press.
12. Whitham, G.B., Linear and Nonlinear Waves. Linear and Nonlinear Waves. 1999. i-xvii.
13. Cavaleri, L. and P. Malanotte-Rizzoli, Wind wave prediction in shallow water: Theory and applications. Journal of Geophysical Research, 1981. 86(C11): p. 10961-10973.
14. Group, T.W., The WAM Model—A Third Generation Ocean Wave Prediction Model. Journal of Physical Oceanography, 1988. 18(12): p. 1775-1810.
15. Wu, J., Wind-stress coefficients over sea surface from breeze to hurricane. Journal of Geophysical Research: Oceans, 1982. 87(C12): p. 9704-9706.